On damping characteristics of frictional hysteresis in pre-sliding range

Michael Ruderman* and Makoto Iwasaki**

* Department of Engineering Sciences
University of Agder, 4879 Grimstad, Norway
** Department of Computer Science and Engineering
Nagoya Institute of Technology, 466-8555 Nagoya, Japan

E-mail: michael.ruderman@uia.no

Abstract. Frictional hysteresis at relative motion in the pre-sliding range is considered. This effect is characterized by an elasto-plastic interaction, and that on the micro-scale, between two rubbing surfaces in contact that gives rise to nonlinear friction force. The pre-sliding friction force yields hysteresis in displacement. In this study, the damping characteristics of frictional hysteresis are analyzed. It is worth noting that we exclude the viscous damping mechanisms and focus on the pure hysteresis damping to be accounted in the friction modeling. The general properties of pre-sliding friction hysteresis are demonstrated and then compared with the limit case of discontinuous Coulomb friction. Further we consider two advanced dynamic friction models, LuGre and Maxwell-slip, so as demonstrate their damping properties and convergence of the motion system to equilibrium state. Experimental observations of the free motion in pre-sliding range are also shown and discussed.

1. Introducing remarks

The frictional hysteresis in pre-sliding range is one of the least understood phenomena of kinetic friction in mechanical systems. It should be stressed that besides a physics-based tribological study of friction effects (see e.g. [1]), the latter can be equally investigated from the system and control point of view, thus operating with the scalar force and velocity. The earlier works on modeling, analysis, and control methods of friction in machines (see the survey [2] and references therein) already emphasized the significance of pre-sliding friction range and related hysteresis in displacement. The convergence of (PID) controlled motion with Coulomb and static friction and possible appearance of the limit cycles has been studied in [3]. Later, the friction-induced limit cycles have been described and demonstrated in [4] for static and dynamic (LuGre) friction models. Recently the convergence of a feedback-controlled motion has been analyzed in context of pre-sliding hysteresis and evaluated experimentally in [5]. A theoretical analysis of pre-sliding frictional hysteresis acting as a feedback to the moving mass can be found in [6]. The pre-sliding behavior of several state-of-the-art dynamic friction models has been classified and compared in terms of the proposed common metrics (so-called Z-properties chart) in [7]. Further it is worth noting that the system-oriented dynamic friction modeling undergos continuous advancements and refinements which are related to the novel experimental observations on the one hand, and model applicability in control practice on the other hand, see e.g. [1, 8, 9].

In this paper, we analyze the damping characteristics of frictional hysteresis in pre-sliding range and investigate the generic force-displacement hysteresis properties in a vicinity to equilibrium of the free motion after an initial steady-state. Here it is worth noting that the end of a free motion due to nonlinear hysteresis is connatural to an unforced behavior of elastic-plastic oscillators. The earlier works in that direction have been also reported e.g. in [10, 11, 12].

2. General consideration

We start our analysis by considering the unforced one-degree-of-freedom relative motion subject to the Coulomb friction. For the sake of simplicity and without loss of generality we assume a unity mass and unity Coulomb friction coefficient, so that the relative motion in $(y, \dot{y})$-coordinates can be described by the following differential equation

$$\ddot{y} = -\text{sign}(\dot{y}) \, . \tag{1}$$

Introducing the vector field

$$f(\mathbf{x}) = \begin{pmatrix} x_2 \\ -\text{sign}(x_2) \end{pmatrix} \quad \text{with} \quad \mathbf{x} = (x_1, \, x_2)^T \in \mathbb{R}^2 \tag{2}$$

we obtain the state-space representation of system (1) as

$$\begin{pmatrix} \dot{x}_1 \\ \dot{x}_2 \end{pmatrix} = \begin{pmatrix} x_2 \\ -\text{sign}(x_2) \end{pmatrix} \, , \tag{3}$$

which is in relative displacement-velocity coordinates. Since the vector field does not depend on the relative displacement we consider the single-variate Lyapunov function $V(x_2) = 1/2 \, x_2^2$ which constitutes kinetic energy of the moving mass. For the time derivative of Lyapunov function $d/dtV(\mathbf{x}) = \nabla V(\mathbf{x}) f(\mathbf{x})$ one easily obtains

$$\frac{d}{dt} V(x_2) = -|x_2|, \tag{4}$$

which implies that

$$\forall \, x_2 \neq 0 \quad \frac{d}{dt} V(x_2) < 0.$$

Since $V(x_2)$ is radially unbounded, the inequality above proves the global system stability in Lyapunov sense, and one can conclude that any unforced motion trajectory, i.e. starting at any point $\{\mathbf{x} : x_2 \neq 0\}$, will approach the equilibrium set $E = \{\mathbf{x} \in \mathbb{R}^2 : x_2 = 0\}$ in finite time. For equilibrium set E at zero velocity, which is a discontinuity manifold due to the sign-operator of Coulomb friction, we proceed similar to [13] by applying the invariance principle, also known as LaSalle's invariance principle (see e.g. [14] for details). The discontinuity manifold E divides the total phase plane P into two regions $P^+ = \{\mathbf{x} \in \mathbb{R}^2 : x_2 > 0\}$ and $P^- = \{\mathbf{x} \in \mathbb{R}^2 : x_2 < 0\}$. At each discontinuity point $\mathbf{x}_e \in E$ the vector field is oriented in opposite directions and is normal to the x_1-axis that follows from

$$f^+(\mathbf{x}_e) = \lim_{\mathbf{x} \to \mathbf{x}_e, \, \mathbf{x} \in P^+} f(\mathbf{x}) = \begin{pmatrix} 0 \\ -1 \end{pmatrix} \, , \tag{5}$$

$$f^-(\mathbf{x}_e) = \lim_{\mathbf{x} \to \mathbf{x}_e, \, \mathbf{x} \in P^-} f(\mathbf{x}) = \begin{pmatrix} 0 \\ +1 \end{pmatrix} \, . \tag{6}$$

Therefore, it can be concluded that once a trajectory reaches the x_1-axis it stays there forever. This is a significant issue since it shows that the Coulomb friction does not only provide a

constant damping rate at unidirectional motion, i.e. according to $|\ddot{y}| = const$, but equally ensures an equilibrium state once reaching zero velocity.

Now, we are to analyze the friction hysteresis in displacement which is known to occur within a micro-displacement range, often denoted as pre-sliding range or pre-sliding region, each time the motion direction changes. Assuming the total friction force at an unidirectional steady-state motion is captured by the Coulomb friction[1] $F = \text{sign}(\dot{y})C$, where $C > 0$ is the Coulomb friction coefficient, we focus on the friction force transitions in a vicinity to motion reversals. Consider the friction trajectories in the force-displacement coordinates as depicted in Figure 1. Let us discuss in details and compare with each other three principally different reversal transitions as these are sketched in the figure.

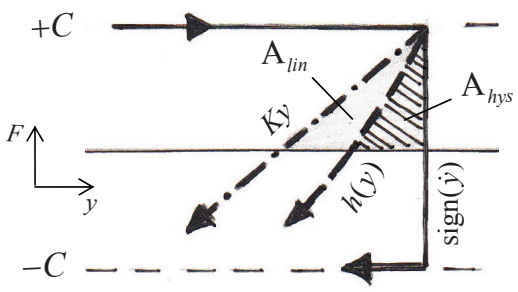

Figure 1. Friction-displacement curves after a motion reversal. The case of elastic contacts with linear stiffness is denoted by Ky, of hysteresis transition by $h(y)$, and the limit case of Coulomb friction is denoted by $\text{sign}(\dot{y})$. The shaded and scratch-through areas, A_{lin} and A_{hys} correspondingly, represent the energy recuperated at motion reversal in the linear and hysteresis case.

The first reversal transition, denoted by Ky, represents a purely elastic case with linear stiffness K of frictional contacts. It should be noted that the combination of steady-state Coulomb friction and Ky reversal transitions yields the behavior of classical Maxwell-slip element, as it will be addressed in details in Section 3.2 when discussing the Maxwell-slip friction model. Recall that in the transition characteristics the Maxwell-slip element coincides with the stop-type Prandtl-Ishlinskii operator. For more details on the latter we refer to e.g. [15], [16].

The next reversal transition, denoted by $h(y)$, is of hysteresis type. Without assuming a particular analytical form, the $h(y)$ function can be imposed on the certain (general) properties which should be fulfilled in order to map the pre-sliding hysteresis friction:

(a) the function $h(y)$ is defined on the interval $[y_r, y_r + \text{sign}(\dot{y})s]$ where y_r is the recent reversal point and $s > 0$ is a finite constant characterizing the recent pre-sliding range;

(b) the function $h(y)$ is monotonically non-decreasing and continuously differentiable (at least once);

(c) the function $dh(y)/dy$ is non-negative and monotonically non-decreasing if $\dot{y} < 0$ and non-increasing if $\dot{y} > 0$. This yields $h(y)$ convex for $\dot{y} < 0$ and concave for $\dot{y} > 0$;

(d) the function $h(y)$ is bounded by $\max\big|h(y)\big| = C$;

(e) at the domain boundary $y = y_r + \text{sign}(\dot{y})s$ the function $dh(y)/dy = 0$, i.e. $h(y)$ is saturated.

Corollary, the properties (d) and (e) imply that after a pre-sliding range the friction force reaches the Coulomb friction level and remains on that until next motion reversal.

The last reversal transition, denoted in Figure 1 by $\text{sign}(\dot{y})$, corresponds to the Coulomb friction behavior, where the friction force changes stepwise at each motion reversal. This represents a limit case for hysteresis transition when $s \to 0$. It can be seen that the $h(y)$ transition passes into the $\text{sign}(\dot{y})$ one when allowing $s = 0$.

[1] As stated in the Introduction part, the recent work is concerned only with the hysteresis damping characteristics of pre-sliding friction. Therefore, the total friction force F considered here does not include the viscous, Stribeck, and transient (dynamic) effects of kinetic friction.

We are now in a position to analyze the damping characteristics of each reversal transition as in Figure 1. For this purpose consider the unforced motion of a unity mass. The concentrated (point) mass is in contact with a homogenous fixed horizontal surface, so that the assumed one-degree-of-freedom motion is antagonized by the tangential friction force F, thus yielding

$$\ddot{y} = -F(\dot{y}) \,. \tag{7}$$

The case where the total friction force is Coulomb (see eq.(1)) has been already analyzed above, turning out that the damping rate is constant until the abrupt stop, which occurs once reaching zero velocity. Henceforth, let us consider the energy balance at motion reversal for two residual transition cases, i.e. linear case denoted by Ky and hysteresis case denoted by $h(y)$. Note that the recent reversal where the sign($\dot{y}$) changes from "+" to "−" is identical to that from "−" to "+" due to the symmetry. Thus, we discuss the situation as illustrated in Figure 1 without loss of generality. Further, we denote the relative position where the corresponding force curve crosses the y-axis by y_0.

At a motion reversal, the kinetic energy is zero due to $\dot{y} = 0$. However, in case of a linear transition the potential energy $W_{lin} = 1/2\, K(y_r - y_0)^2$ is stored due to elastic contacts with stiffness K. It means that when moving back from y_r to y_0, i.e. after a motion reversal, the total amount of energy is recuperated that corresponds to the area A_{lin} indicated in Figure 1. That allows the system continuing to move into the same direction after crossing zero force, while the magnitude of counteracting friction force will increase according to $F = K(y - y_0)$. Since $y_0 = const$ for each particular reversal at y_r, we introduce the local motion variable $z = y - y_0$ with $\ddot{z} = \ddot{y}$ and obtain the system dynamics at reversal transitions as

$$\ddot{z} = -Kz \,. \tag{8}$$

It is easy to recognize that (8) constitutes an undamped harmonic oscillator for which we have an explicit time-domain solution given by

$$z(t) = Z_0 \cos(\omega t) \quad \text{with} \quad Z_0 = y_r - y_0 \quad \text{and} \quad \omega = \sqrt{K} \,. \tag{9}$$

Important to note is that once launched at Z_0, the friction force oscillator will operate between $\pm Z_0$ without passing again to the Coulomb friction state. This is due to the relative motion is unforced. The motion trajectories in the (y, $\dot{y}$)-plane result in the closed elliptic orbits whose axes depend on the initial state Z_0 and physical parameters, i.e. stiffness and mass. Thus it can be concluded that a purely elastic reversal transition does not provide an asymptotic equilibrium state after reaching zero velocity and, instead of this, induces a stable (linear) limit cycle. This result will be reawakened in Section 3.2 when analyzing damping of the Maxwell-slip friction model.

In case of a hysteresis reversal transition, similar consideration of potential energy stored at a motion reversal can be done, however, with the total amount of recuperated energy $W_{hys} = A_{hys} < A_{lin}$, as obvious from Figure 1. Since the force transition is given by the nonlinear function $h(y)$, the energy balance is determined by $W_{hys}(y) = \int_{y_r}^{y} h(y)dy$ and that until the next motion reversal. In order to provide an analytical solution in the phase-plane we rewrite the system dynamics (7) by using $\ddot{y} = \dot{y}d\dot{y}/dy$ and obtain

$$\dot{y}d\dot{y} = -h(y)dy \,. \tag{10}$$

Integrating (10) with respect to the motion interval, i.e. from y_r to y, yields

$$\int_{y_r}^{y} h(y)dy = -\frac{1}{2}\dot{y}^2\Big|_{\dot{y}_r}^{\dot{y}} \,. \tag{11}$$

Since the velocity sign is a-priori given and the system dynamics (10) is defined between two consecutive motion reversals with $\dot{y}_r = 0$ we can calculate the velocity function as

$$\dot{y}(y) = \mathrm{sign}(\dot{y})\sqrt{2\int_{y_r}^{y} h(y)dy}\,. \tag{12}$$

Inspecting (12) and with respect to the $h(y)$-properties (a)–(e) two significant implications can be drawn.

(i) Since $\left|\int_{y_r}^{y} h(y)dy\right|$ is growing on the interval $[y_r,\, y_0)$ and reducing afterwards, the $\max|\dot{y}|$ value occurs at the y_0 position, i.e. at zero-crossing of friction force. That is the $(y_0,\, \max|\dot{y}|)$ state subdivides each hysteresis transition into an acceleration and deceleration phase.

(ii) At the next motion reversal y_r^+ which occurs after the relative velocity becomes again zero $\dot{y}_r^+ = 0$, according to (12), the magnitude of friction force decreases comparing to that of previous reversal, i.e. $\left|h(y_r^+)\right| < \left|h(y_r)\right|$. This follows from the property (c) of hysteresis function $h(y)$ and implies that the potential energy, which can be recuperated after next motion reversal, is lower than that after the previous motion reversal, i.e. $W_{hys}(y_r^+) < W_{hys}(y_r)$.

From implication (ii) it can be concluded that each hysteresis transition dissipates the energy and the motion system (7) attains a stable equilibrium state $(y_r^i, \dot{y}_r^i = 0)$ at the finite number of reversals $i > 1$. As corollary, we can note that the equilibrium state lies always between the first and second reversal point, i.e. $\min(y_r^\infty, y_r^\in) \leq y_r^i \leq \max(y_r^\infty, y_r^\in)$. Further, it is worth noting that at the reached equilibrium state the residual (stiction) friction force is not necessarily zero and can comply with $0 \leq |F(\dot{y}_r^i = 0)| < C$. This corresponds to adhesion mechanisms of the static (stiction) friction and is out of scope in the recent study. The single explanation, to be given here, on non-zero friction at the reached motion equilibrium is that it can be considered as a Coulomb-like friction behavior where $F(\dot{y}_r^i) = \mathrm{sign}(\dot{y})c$ with $0 < c < C$. This ensures the system remains sticking in the attained equilibrium even if $F \neq 0$, as has been analyzed at the beginning of this Section. Further we note that reaching a stable equilibrium at $i = 1$ corresponds to the Coulomb friction transition $\mathrm{sign}(\dot{y})$ which has been analyzed beforehand.

For the analysis accomplished above we are to demonstrate the unforced motion trajectories, and that for all three reversal transitions. The results are obtained by means of a numerical simulation. For the sake of simplicity we assume the unity mass, unity linear stiffness, and unity Coulomb friction coefficient. In case of hysteresis reversal transition we apply the LuGre friction model, addressed further in Section 3.1. The unforced motion trajectories with an initial state $(y, \dot{y})(0) = (0, 5)$ are shown in the phase-plane in Figure 2 for all three cases. It can be seen that the trajectories confirm the analysis made above.

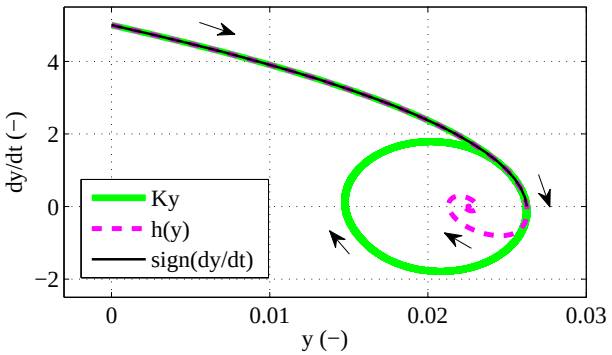

Figure 2. Unforced motion trajectories starting from an initial state $(y, \dot{y})(0) = (0, 5)$. The Coulomb reversal transition provides a stable convergence without transient oscillations. The linear reversal transition results in a stable limit cycle within pre-sliding range. The hysteresis reversal transition yields the nonlinearly-damped (oscillating) transient towards a stable equilibrium.

3. Hysteresis damping in friction models

In this Section we consider two advanced dynamic friction models, i.e. LuGre and Maxwell-slip, and analyze their damping characteristics when mapping the pre-sliding friction range. The selection of friction models for analysis is not influenced by any particular preference and solely bases on their quite different formulation and widespread use in structural mechanics and control. The *LuGre* model [17], which is most widespread in control, extends the Dahl[2] model (see [18], [19] for details) by including the damping of internal (pre-sliding) friction state and allowing for more complex, than only Coulomb, steady-state friction characteristics, i.e. the so-called Stribeck effect. The LuGre friction model incorporates also the viscous friction term which is, however, omitted in the recent study since we are only focusing on the damping characteristics of hysteresis. The *Maxwell-slip* model, or more generally Maxwell-slip structure, is suitable for describing any rate-independent hysteresis between the generalized motion and forces, see e.g. [20] for details. The approach was equally used for modeling the hysteresis behavior of materials and structures in [21], and in particular of piezoelectric stacks in [22]. It should be stressed that the parallel connection of single elasto-slip Maxwell elements renders a structure which replicates the Prandtl-Ishlinskii stop-type hysteresis model, see e.g. [15] for details. In the following Subsections, each friction model is briefly summarized for convenience of the reader. Afterwards, the analysis of damping behavior in vicinity to an equilibrium, i.e. motion stop, is performed for each model when incorporated in the system dynamics (7).

3.1. LuGre model

The LuGre friction model captures the total tangential friction force

$$F(\dot{y}) = \sigma_0 z + \sigma_1 \dot{z} + \sigma_2 \dot{y} \tag{13}$$

as a linear combination of internal friction state z, its damping, and viscous friction term which depends on the relative velocity. The positive parameters σ_0 and σ_1 can be understood as the contact stiffness and micro-damping correspondingly. The non-negative viscous friction coefficient is σ_2. Often, the internal state z is associated with the so-called 'bristle' (or also 'brush') model of frictional interaction of asperities which form the contacting surfaces, as schematically shown in Figure 3 (cf. with [23], [17]). A large number of bristles (with a rather statistical distribution and thus average lengths and distances) deflect like the springs (not necessarily linear) at a relative motion. Thus, the internal state z can be seen as an average deflection of the bristles until a steady motion sets on.

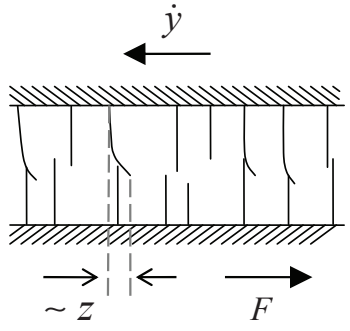

Figure 3. Schematic representation of two sliding surfaces in contact by means of so-called bristle (also brush) friction model. The tangential friction force F acts in opposite direction to the relative motion $\dot{y}$. The internal friction state z is associated with an average deflection of bristles.

[2] The Dahl model was, probably, the first trial to extend the Coulomb friction law so as to resolve the discontinuity at motion reversals. The Dahl model introduced an internal state to describe the reversal transition of friction force, thus capturing the pre-sliding hysteresis. The model was long time a standard approach in the aero-space industry to describe friction behavior in the ball-bearing type mechanisms.

The internal friction state is governed by

$$\dot{z} = \dot{y} - \sigma_0 \frac{|\dot{y}|}{g(\dot{y})} z, \tag{14}$$

where the positive nonlinear static map $g(\cdot)$ captures the Coulomb friction and Stribeck effect. In the following, however, we consider $g = C$ only so as to be in accord with the previous assumptions and hence to exclude other steady-state friction components than the Coulomb friction. For the same reason, we require $\sigma_2 = 0$ so that no viscous friction behavior will be taken into account as mentioned before.

At this stage, some significant properties and parameter conditions posed on the LuGre friction model, and known from the literature, should be briefly mentioned with respect to the dissipative nature of friction. The necessary and sufficient conditions for passivity of the LuGre friction model have been investigated in [24] and a strict, but quite simple at the same time, inequality has been derived in terms of the model parameterization. It postulates the input-output (I/O) dissipativity of an $\dot{y} \mapsto F$ map if and only if (see Property 3 in [19])

$$\sigma_2 > \sigma_1 \frac{F_s - C}{C} \,, \tag{15}$$

where $F_s \geq C$ corresponds to the stiction force, which is considered for mapping the Stribeck effect (in the original LuGre model). We can note that even if $(F_s - C) \to 0$ the viscous damping $\sigma_2 \neq 0$ is required for rendering the LuGre model I/O dissipative. Since no viscous damping is assumed in the recent study neither straightforward conclusions on passivity, and furthermore stability, of a frictional system can be drown based on the analysis provided in [24], [19].

With assumptions made above on the steady-state friction and viscous damping the total friction force described by the LuGre model becomes

$$F(\dot{y}) = \sigma_1 \dot{y} + \sigma_0 \Big(1 - \sigma_1 \frac{|\dot{y}|}{C}\Big) z \,. \tag{16}$$

Therefore, the unforced motion dynamics (7) can be written in the state-space form

$$[\dot{z}, \ddot{y}]^T = A(\dot{y})[z, \dot{y}]^T \,, \tag{17}$$

with the state-dependent system matrix

$$A(\dot{y}) = \begin{pmatrix} -\sigma_0 \frac{|\dot{y}|}{C} & 1 \\ -\sigma_0 \Big(1 - \sigma_1 \frac{|\dot{y}|}{C}\Big) & -\sigma_1 \end{pmatrix} . \tag{18}$$

To be able to make a statement about the damping characteristics of system (17), (18), or generally first of all about its stability, the linearization of (18) should be made. However, this requires inspecting the total domain of velocity magnitudes which can render our analysis cumbersome. Furthermore, no particular operating points of $|\dot{y}|$ can be identified so as to perform a reasonable linearization. In fact, we are rather interested in the transient dynamics of system (17), (18), i.e. after the first motion reversal and until the final motion stop. The single particular state which is appropriate for linearization is $\dot{y} \to 0$. This is a boundary case close to the motion reversal or final motion stop. Here the system matrix becomes

$$A(0) = \lim_{\dot{y} \to 0} A(\dot{y}) = \begin{pmatrix} 0 & 1 \\ -\sigma_0 & -\sigma_1 \end{pmatrix} . \tag{19}$$

It is evident that for any $\sigma_0 > 0$ and $\sigma_1 > 0$ the eigenvalues of $A(0)$ are in the left-half complex plane and the linearized system is asymptotically stable. This is well in accord with the results of linearization in the so-called stiction regime of LuGre friction model which have been provided in the original work [17]. The damping characteristics are fully determined by the σ_0 and σ_1 parameters. For the critically-damped solution of characteristic polynomial of matrix $A(0)$ one can show that if $\sigma_1 < 2\sqrt{\sigma_0}$ the system has an oscillating behavior. That means multiple motion reversals should occur before reaching the final equilibrium state.

In order to prove a stable convergence of system (17), (18) we apply the Aiserman's method [25] of finding a suitable Lyapunov function candidate $V(z, \dot{y})$ and evaluating its time derivative. The system matrix (18) can be split into the constant (state-independent) and variable (state-dependent) terms as

$$A(\dot{y}) = A_0 + \tilde{A}(\dot{y}) = \begin{pmatrix} 0 & 1 \\ -\sigma_0 & -\sigma_1 \end{pmatrix} + \begin{pmatrix} -f(\dot{y}) & 0 \\ \sigma_1 f(\dot{y}) & 0 \end{pmatrix}, \tag{20}$$

where $f(\dot{y}) = \sigma_0|\dot{y}|/C > 0$ for all $\dot{y} \neq 0$. We assume the positive definite (p.d.) matrix

$$P = \begin{pmatrix} \sigma_0 & 0 \\ 0 & 1 \end{pmatrix} \tag{21}$$

that yields a p.d. Lyapunov function candidate $V = (z, \dot{y})P(z, \dot{y})^T$, which is radially unbounded since $V \to \infty$ as $\|(z, \dot{y})\| \to \infty$. Now, evaluating the Lyapunov equation for the constant part of the system matrix one obtains

$$Q_0 = -A_0^T P - P A_0 = \begin{pmatrix} 0 & 0 \\ 0 & 2\sigma_1 \end{pmatrix}. \tag{22}$$

It can be seen that for a positive micro-damping σ_1 the matrix Q_0 is positive semi-definite (p.s.d.) so that the corresponding part of derivative of the Lyapunov function candidate

$$\dot{V}_0(z, \dot{y}) = -(z, \dot{y})Q_0(z, \dot{y})^T \leq 0 \tag{23}$$

is negative semi-definite (n.s.d.) only. This is quite natural since for $\dot{V}_0 = -2\sigma_1\dot{y}^2$ no impact of the z-dynamics can be taken into account and evaluated. In fact, the $\dot{V}_0 = 0$ for $\dot{y} = 0$ does not necessary imply that $z = 0$. For the state-dependent part of the system matrix the corresponding Lyapunov equation yields

$$\tilde{Q}(\dot{y}) = -\tilde{A}^T(\dot{y})P - P\tilde{A}(\dot{y}) = \begin{pmatrix} 2f(\dot{y})\sigma_0 & -f(\dot{y})\sigma_1 \\ -f(\dot{y})\sigma_1 & 0 \end{pmatrix} \equiv \begin{pmatrix} 2\sigma_0 & -\sigma_1 \\ -\sigma_1 & 0 \end{pmatrix}. \tag{24}$$

Note that the last (equivalence) transformation in (24) is due to the positive $f(\cdot)$ for all $\dot{y} \neq 0$. The obtained (partial) solutions of both Lyapunov equations, i.e. (22) and (24), allow constructing the derivative of the total Lyapunov function candidate as

$$\dot{V} = \dot{V}_0(z, \dot{y}) - (z, \dot{y})\tilde{Q}(\dot{y})(z, \dot{y})^T = -2\sigma_1\dot{y}^2 - 2\sigma_0 z^2 + 2\sigma_1 z\dot{y} \equiv -\dot{y}^2 - \frac{\sigma_0}{\sigma_1}z^2 + z\dot{y}. \tag{25}$$

For $\dot{V}$ to be negative definite (n.d.) the ellipsoid inequality

$$\dot{y}^2 + \frac{\sigma_0}{\sigma_1}z^2 > z\dot{y} \tag{26}$$

should hold $\forall\, z \in \mathbb{R}, y \in \mathbb{R}$. Here it is worth noting that the internal friction state z is bounded. This has been explicitly addressed and shown in [19] (see Property 1 therein). Nevertheless,

for the sake of simplicity, we do not account for this auxiliary condition. It is evident that (26) holds always when $\text{sign}(z) \neq \text{sign}(\dot{y})$. This corresponds to all the intervals $[y_r, y_0]$, i.e. after a motion reversal and until zero-crossing of hysteresis transition curve (see Section 2). For $\text{sign}(z) = \text{sign}(\dot{y})$ we prove the solution of equality $\dot{y}^2 + \sigma_0/\sigma_1 z^2 = z\dot{y}$, which is

$$z = \frac{\sigma_1}{2\sigma_0}\Big(\dot{y} \pm \dot{y}\sqrt{-\frac{4\sigma_0 - \sigma_1}{\sigma_1}}\Big). \tag{27}$$

It is evident that for equation (27) obtains a real solution, the following parameter condition

$$\sigma_0 < \frac{\sigma_1}{4} \tag{28}$$

should hold. Otherwise, no real solutions of friction state z are existing and we can conclude that the inequality (26) holds everywhere in the state-space. This yields $\dot{V}$ to be n.d. and ensures a stable system convergence to the $(z, \dot{y}) = \mathbf{0}$ equilibrium. In case when however (28) holds, there are regions in the state-space where $\dot{V}$ is not n.d. and the system becomes unstable in the Lyapunov sense. Though, we will not analyze this case in more details since for real physical systems the parameter relation (28) appears as improper. Recall that σ_0 corresponds to the stiffness and σ_1 to the micro-damping of frictional contacts. Hence, in almost all physically-reasonable friction systems $\sigma_0 \gg \sigma_1$.

It is intuitively reasonable that higher micro-damping, i.e. higher σ_1 values, provides a faster convergence towards the equilibrium. This implies (indirectly) a lower number i of motion reversals until the relative motion will fully stop. However, an interesting fact occurs when allowing even zero micro-damping, i.e. $\sigma_1 = 0$. In that case one can easily show that the resulted system matrix

$$\hat{A}(\dot{y}) = \begin{pmatrix} -\sigma_0 \frac{|\dot{y}|}{C} & 1 \\ -\sigma_0 & 0 \end{pmatrix} \tag{29}$$

is n.d. for all $y \neq 0$. This yields the system asymptotically stable at hysteresis transitions and marginally stable at zero velocity, i.e. at motion reversals. Also when assuming a related Lyapunov function candidate

$$\hat{V} = \frac{1}{2}\dot{y}^2 + \frac{1}{2}\sigma_0 z^2 \tag{30}$$

one can easily obtain

$$\dot{\hat{V}} = -\sigma_0^2 \frac{|\dot{y}|}{C} z^2 \tag{31}$$

which is n.d. in the whole state-space. This yields the system asymptotically stable even if zero micro-damping is assumed.

3.2. Maxwell-slip model

The Maxwell-slip friction model can be well understood by means of the associated Maxwell-slip structure as depicted in Figure 4. The latter contains N parallel-connected elasto-plastic (or elasto-slip) Maxwell elements which are either sticking or slipping. When the j-th element is subject to the (common) input velocity $\dot{y}$ the linear spring with stiffness k_j is elongating as long as $k_j|y| \leq c_j$. Once the spring force exceeds the individual breakaway force c_j, the element begins to slip and that until the next motion reversal. It is worth noting that all the slipping blocks are assumed as massless so that no dynamic interaction occurs during their relative motion. The associated output friction force (of each block) is $F_j = k_j y$ when sticking and $F_j = c_j \text{sign}(\dot{y})$

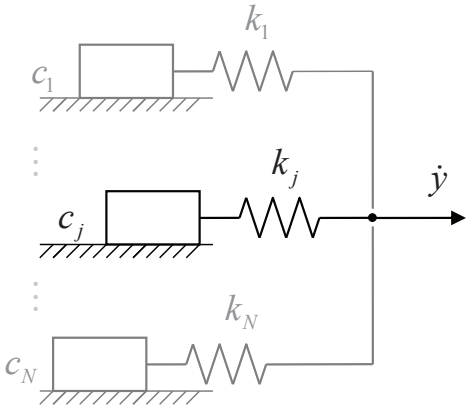

Figure 4. Maxwell-slip structure of N parallel-connected elasto-slip (Maxwell) elements. Each j-th element is characterized by ist individual stiffness $k_j > 0$ and breakaway force $c_j > 0$. The elements are driven by the common velocity input $\dot{y}$. Each element is sticking during the relative spring elongation, i.e. while $k_j|y| \leq c_j$. Afterwards the element is slipping, with a constant counteraction $c_j \mathrm{sign}(\dot{y})$, until the next motion reversal.

when slipping (compare with Ky reversal transition in Section 2). Due to a parallel connection of the blocks the total friction force is

$$F(\dot{y}) = \sum_{j=1}^{N} F_j \,. \tag{32}$$

In order to analyze the system dynamics (7) when using the Maxwell-slip friction model, we are to consider each elasto-slip Maxwell element by means of the play- and stop-type hysteresis operators (see [15], [26], [27] for details). Recall that an elasto-slip Maxwell element offers the same transfer characteristics as the stop-type hysteresis operator. To that end, the stop-type hysteresis operator can be constructed by means of his play-type counterpart. The transfer characteristics of a play-type hysteresis operator $x = \mathcal{P}(r, x_0)[y]$ are shown in Figure 5. The operator provides a multi-valued rate-independent map $y \mapsto x$ depending on the initial state x_0 and parameter r. The latter determines, as can be seen from Figure 5, the width of the play zone which equals $2r$. One can realize that each time the input direction changes, the operator is in the play zone until reaching the corresponding slope $y - \mathrm{sign}(\dot{y})r$. Within the play zone the output remains constant while keeping its previous value. The operator dynamics in differential form, of which later we will make use, is given by

$$\dot{x} = \begin{cases} \dot{y} & \text{if } \; x - r = y \;\vee\; x + r = y \,, \\ 0 & \text{if } \; x - r < y < x + r \,. \end{cases} \tag{33}$$

In the following, and that for the sake of simplicity, we will write the play-type hysteresis

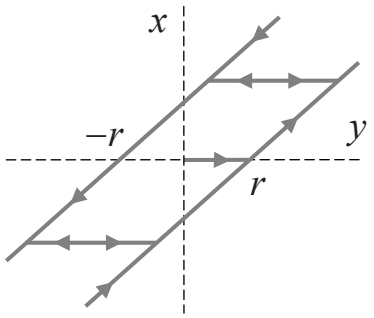

Figure 5. Transfer characteristics of rate-independent play-type hysteresis operator $\mathcal{P}$, also known as mechanical backlash. The play-type hysteresis operator $x = \mathcal{P}(r, x_0)[y]$ is parameterized by the width of the play zone $2r$. Each time the input direction changes, the operator enters the play zone in which the output remains constant while keeping its previous value.

operator by a functional notation $x(y, r)$.

The unique property of a stop-type hysteresis operator is that this can be transformed from its play-type counterpart by the simple algebraic relation $y - x(y, r)$. This allows constructing the single elasto-slip Maxwell element as

$$F_j = k_j\big(y - x(y, r_j)\big)\,, \tag{34}$$

when tacking into account the corresponding parameterization $r_j = c_j/k_j$. Recall that the closed form (34) is rate-independent and represents the hysteresis transition, in relative force-displacement coordinates, between the element sticking and slipping and vice versa.

Now, we are in a position to analyze the convergence of free motion (7), and therefore the damping characteristics of pre-sliding hysteresis, when assuming the friction force (32). For the sake of clarity we are first exploring the case $N = 1$, i.e. when a single elasto-slip Maxwell element is assumed. Afterwards, we generalize our analysis to the case $N > 1$ and discuss a limit case when $N \to \infty$. We note that the case $N = 1$ corresponds to the linear reversal transition which has been indicated by Ky and discussed before in Section 2. Here, however, we are to establish a Lyapunov-based analysis so as to make it further extendable for a general multi-element Maxwell-slip structure.

The single elasto-slip Maxwell element yields the free motion dynamics as

$$\ddot{y} = -k_1 y + k_1 x(y, r_1)\,. \tag{35}$$

Since the hysteresis operator can accumulate, or eventually release, the energy in the system, we introduce an internal state $z = x - y$, which is bounded by $-r_1 \le z \le r_1$, and apply the Lyapunov function candidate

$$V(\dot{y}, z) = \frac{1}{2k_1}\dot{y}^2 + \frac{1}{2}z^2. \tag{36}$$

Note that V is p.d. and radially unbounded since $V \to \infty$ as $\|(\dot{y}, z)\| \to \infty$. The time derivative of the Lyapunov function candidate results in

$$\dot{V} = \dot{y}z + \dot{z}z, \tag{37}$$

which is case-specific depending on whether the element is sticking or slipping. Here it should be noted that two cases correspond to the play zones and slopes of the play-type hysteresis operator (see Figure 5). From the internal state dynamics $\dot{z} = \dot{x} - \dot{y}$ point of view and with respect to (33) we can emphasize that $\dot{z} = 0$ when operating on one of the slopes, and $\dot{z} = -\dot{y}$ when operating within a play zone. This renders the time derivative of Lyapunov function candidate as

$$\dot{V} = \begin{cases} \dot{y}z & \text{for } \dot{x} = \dot{y} \ \text{(slope)}, \\ 0 & \text{for } \dot{x} = 0 \ \text{(play zone)}. \end{cases} \tag{38}$$

It can be seen from Figure 5 that the right-hand side slope, i.e. $\dot{y} > 0$, implies $z = -r$, and the left-hand side slope, i.e. $\dot{y} < 0$, implies $z = r$ correspondingly. Therefore, we can conclude that when operating on a slope the inequality $\dot{y}z < 0$ always holds. The latter renders $\dot{V}$ as n.d. and implies the system is globally asymptotically stable in the Lyapunov sense when slipping. On the contrary, within a play zone where $\dot{V} = 0$ the system yields marginally stable, but not asymptotically stable, in the Lyapunov sense. Here the system moves along the closed elliptic trajectories as has been analyzed before in Section 2.

Since the total time derivative of Lyapunov function candidate is n.s.d. only, i.e. $\dot{V} \le 0$, we are to show that there exists an invariant set which consists of the stable linear limit cycles during the system sticking. Applying the invariant set theorem (see [14] for details), we assume

for some $l = 1/2r^2 + a > 0$ the region Ω defined by $V(\dot{y}, z) < l$ which is bounded. In fact, since z is bounded by $\pm r$, and further with respect to (36), one can see that Ω is bounded on the $\pm\dot{y}$-axis by the constant $a > 0$ which is related to initial velocity. Also it is valid that $\dot{V}(\dot{y}, z) \leq 0$ for all $(\dot{y}, z) \in \Omega$. Now, we have to show that for the set $R \subset \Omega$, which is the largest invariant set with $\dot{V}(\dot{y}, z) = 0$, any trajectory with $\big(\dot{y}(0), z(0)\big) \in \Omega$ tends to R as $t \to \infty$. According to (38), zero derivative $\dot{V} = 0$ corresponds to a play zone of play-type hysteresis operator for which $\dot{x} = 0$. It should be noted that the set of all play zones is infinite and corresponds to the whole horizontal axis of relative position y. For any play zone the corresponding x-value is constant and the motion dynamics (35) becomes

$$\ddot{y} - k_1 z = 0\,. \tag{39}$$

Since $\dot{y} = -\dot{z}$ and $\ddot{y} = -\ddot{z}$ we transform the motion dynamics (39) into the relative z-coordinates and obtain the free motion of sticking system as

$$\ddot{z} + k_1 z = 0. \tag{40}$$

Note that the same result we obtained in Section 2 (see equation (8)). It is obvious that the $(\dot{y}, z)$ solutions constitute the closed elliptic trajectories of limit cycles whose union is the invariant set R. It is worth to recall that for any initial velocity $\dot{y}(0) \neq 0$, i.e. the system is in slipping, the internal state is $z = -\text{sign}(\dot{y})r$, and the play-type hysteresis operator proceeds along one of the slopes until the next motion reversal. Further we stress that for any initial state in Ω with $0 < l \leq 1/2r^2$ the trajectory $(\dot{y}, z)(t) \in R$ for all $t \geq 0$. Here the axes of elliptic limit cycles depend on the initial state $(\dot{y}, z)(0)$. For any initial state with $l > 1/2r^2$ the trajectory first proceeds towards the corresponding $z = -\text{sign}(\dot{y})r$ boundary, i.e. depending on the initial $\dot{y}(0)$ value, and afterwards slides along this boundary until the next motion reversal occurs. The motion trajectories with different initial states are shown in the $(\dot{y}, z)$ plane in Figure 6.

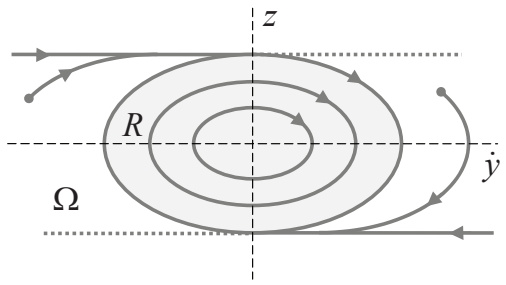

Figure 6. Trajectories of the system (35) in the $(\dot{y}, z)$ plane. The trajectories starting within R form the elliptic limit cycles. The trajectories starting in Ω outside of R first run towards the corresponding $z = -\text{sign}(\dot{y})r$ boundary and then proceed to the next motion reversal. Afterwards, the boundary (largest) limit cycles occurs.

Now, we are to generalize our analysis made above for the case when $N > 1$, therefore incorporating a multi-element Maxwell-slip structure when describing the friction force. The corresponding free motion dynamics results in

$$\ddot{y} = -\sum_{j=1}^{N} k_j y + \sum_{j=1}^{N} k_j x_j(y, r_j), \tag{41}$$

which reduces to (35) when $N = 1$. Introducing the $N \times 1$ vectors of contact stiffness $\mathbf{k} = [k_1, \ldots, k_N]^T$, play-type hysteresis operators $\mathbf{x} = [x_1, \ldots, x_N]^T$ which are parameterized by $\mathbf{r} = [r_1, \ldots, r_N]^T$, and absolute positions $\mathbf{y} = y[1, \ldots, 1]^T$ we rewrite the system dynamics (41) into the vector form

$$\ddot{y} = -\mathbf{k}^T\mathbf{y} + \mathbf{k}^T\mathbf{x}(y, \mathbf{r}). \tag{42}$$

Further we introduce, similar as in case of single Maxwell-slip element, the vector of internal states $\mathbf{z} = \mathbf{x} - \mathbf{y}$ which captures the individual transitions of play-type hysteresis operators. Defining the p.d. diagonal matrix $\tilde{\mathbf{K}} = \mathrm{diag}(k_1, \ldots, k_N)$ we assume the Lyapunov function candidate

$$\tilde{V}(\dot{y}, \mathbf{z}) = \frac{1}{2}\dot{y}^2 + \frac{1}{2}\mathbf{z}^T\tilde{\mathbf{K}}\mathbf{z}, \tag{43}$$

which is p.d. and radially unbounded since $\tilde{V} \to \infty$ as $\|(\dot{y}, \mathbf{z})\| \to \infty$. It can be noted that the Lyapunov function candidate (43) contains the kinetic energy of the free motion and potential energy associated with each hysteresis operator, i.e. elasto-slip Maxwell element. The time derivative of the Laypunov function candidate results in

$$\dot{\tilde{V}} = \dot{y}\mathbf{k}^T\mathbf{z} + \dot{\mathbf{z}}^T\tilde{\mathbf{K}}\mathbf{z}. \tag{44}$$

With respect to the transfer characteristics of each play-type hysteresis operator (see Figure 5 and equation (38)), and herewith associated behavior of single elasto-slip Maxwell element, one can show that

$$\dot{\tilde{V}} = \begin{cases} \dot{y}\mathbf{k}^T\mathbf{z} < 0 & \text{if all } N \text{ elements are slipping,} \\ \dot{y}\mathbf{k}^T\mathbf{z} - \dot{\mathbf{y}}^T\tilde{\mathbf{K}}\mathbf{z} = 0 & \text{if all } N \text{ elements are sticking.} \end{cases} \tag{45}$$

It is easy to recognize that (45) constitutes a boundary case where all play-type hysteresis operators are either on a slope or in a play zone. However, since we are interested in analyzing the case when the system is not asymptotically stable but proceeds in a limit cycle, i.e. when $\dot{\tilde{V}} \equiv 0$, the second case of (45) provides us with the required (strict) condition. In fact, the trajectory is within invariant set R if and only if all N play-type hysteresis operators are in a play zone. In order to prove this, one can easily show that when at least one operator j is on a slope, the corresponding element has $\dot{\mathbf{z}}^T(j) = 0 \neq -\dot{\mathbf{y}}^T(j)$ and its contribution to (44), which is

$$\dot{y}\mathbf{k}^T(j)\mathbf{z}(j) + \dot{\mathbf{z}}^T(j)\tilde{\mathbf{K}}(j,j)\mathbf{z}(j) < 0\,,$$

renders $\dot{\tilde{V}}$ as n.d. Thus, one can conclude that it is sufficient that at least one element is slipping so as the overall system becomes asymptotically stable, and therefore converges to the motion equilibrium $\dot{y} = 0$.

Now, we can analyze whether and when the condition derived above satisfies the pre-sliding system behavior, in particularly in view of hysteresis reversal transitions addressed before in Section 2. While $h(y)$ should be continuously differentiable (see property (b) in Section 2), the friction force (32) constitutes only a piecewise differentiable approximation of $h(y)$. In fact, a force-displacement hysteresis branch described by (32) is a piecewise linear curve with the break points which characterize the sticking-slipping transitions of single elasto-slip Maxwell elements. Since the elasto-slip Maxwell elements are acting in parallel, each slope segment of the piecewise linear curve appears as a superimposed stiffness of all elements which are (still) sticking. At the same time, it should be stressed that immediately after each motion reversal all elements are sticking. Afterwards, they switch one by one to slipping, and that depending on their individual k_j and c_j parameters, while proceeding along the $h(y)$ curve. Therefore, one can conclude that higher numbers N approximate the $h(y)$ function with higher accuracy and, at the same time, provoke more frequent switching from sticking to slipping along the $h(y)$ curve. This implies $r_{k+1} - r_k \to 0$ as $N \to \infty$, where k and $k+1$ are two arbitrary elements whose switching occur successively. Hence, for any element $j = 1$, which switches as first after a motion reversal, $r_1 \to 0$ as $N \to \infty$. With respect to condition of the negative definiteness of $\dot{\tilde{V}}$, derived above, we can conclude that $\dot{\tilde{V}} \to$ n.d. as $N \to \infty$, and that over the whole $(\dot{y}, \mathbf{z})$ state-space. As corollary, one can show that the invariant set contains only the equilibrium point, i.e. $R \to \mathbf{0}$, as $N \to \infty$ (cf. with Figure 6).

4. Experimental observations

In this Section we show and discuss some experimental observations in favor of the analysis of pre-sliding frictional hysteresis made above. The experimental data of a measured motion response are obtained from an actuated rotary system with mechanical friction interfaces. The relative angular displacement y and velocity $\dot{y}$ are measured using a precise digital encoder mounted on the rotary shaft. The overall moving mass (inertia) is axially-symmetrical and assumed to be homogenous and lumped. The feed actuation torque u allows driving the system at certain constant (also low) velocity and can be switched off stepwise, so as to realize (afterwards) a free motion response towards the equilibrium. The principal configuration of the experimental setup in use is shown in Figure 7. Most notable is that the multiple mechanical frictional interfaces can be considered as an aggregated one due to the stiff relative motion within the same rotary degree-of-freedom y. The experimental data, shown in the following, are real-time and collected

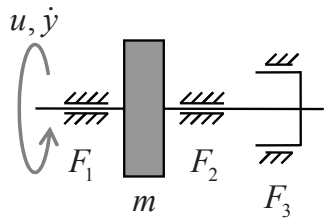

Figure 7. Principal configuration of the experimental actuated rotary system with the lumped moving mass (inertia) m. The frictional interfaces of the ball-bearing F_1, F_2 and gear teething F_3 type are considered as an aggregated friction F, since operating in the same rotary degree-of-freedom. The actuation torque u induces the angular relative displacement with velocity $\dot{y}$.

with the fixed sampling rate of 2 kHz. More details about the used experimental system can be found in [28].

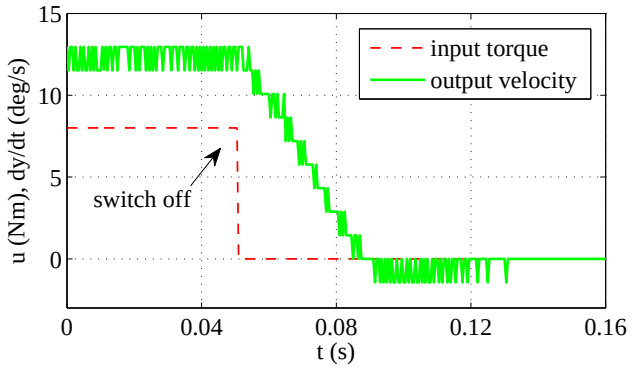

Figure 8. Experimental data of the measured motion response in pre-sliding range. The relative displacement with constant low-velocity is actuated by a constant feed force (torque) until the actuation is switched off. Afterwards, the free system response occurs until the complete motion stop. The nearly linear velocity slope indicates the predominant Coulomb friction and irrelevance of the viscous (exponential) damping.

In Figure 8, the measured motion response is shown as time series together with the corresponding input torque. At a constant torque level the nearly constant relative velocity of about 12.3 deg/s occurs until the actuation is switched off. The irregular high-frequent chattering of the measured velocity is attributed to the sampled and hold (digital) encoder signal and its discrete-time derivation. After the actuation switch off the velocity descends towards zero and the system completely stops after a low transient overshoot. The visible, nearly linear, slope of decreasing velocity indicates a predominance of Coulomb friction (cf. with Section 2) and irrelevance of the viscous (exponential) damping close to the motion stop.

The free motion trajectories are shown in Figure 9 in the $(\dot{y}, y)$ phase-plane. The measured motion response is compared with the model fit of system dynamics once using the LuGre (Figure 9(a)) and once using the Maxwell-slip (Figure 9(b)) friction model. Note that after the actuation switch off the system behavior can be captured by (7) with an appropriately set

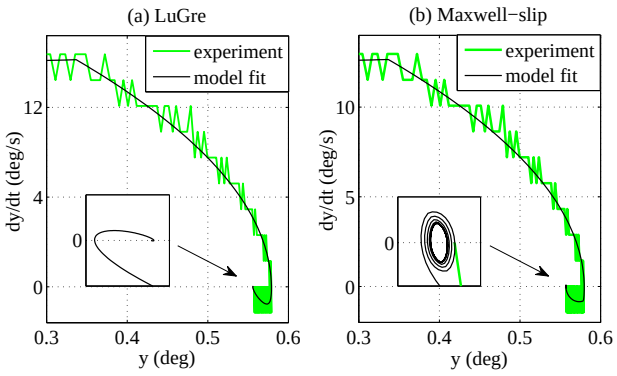

Figure 9. Free motion trajectories in the $(\dot{y}, y)$ phase-plane. Comparison of experimental measurements with the model fit of system dynamics (7) when using the LuGre friction model (a) and Maxwell-slip (with $N = 3$) friction model (b). The model fit is obtained by nonlinear least-squares minimization of the velocity error $\|\dot{\mathbf{y}} - \hat{\dot{\mathbf{y}}}\|$, where $\hat{\dot{\mathbf{y}}}$ is the model-predicted relative velocity. The zoom-in inclusions show the convergence of both models towards equilibrium.

non-zero initial velocity and initial friction $F(0) = \text{sign}(\dot{y})C$. The former is directly determined from the available measurement. The latter is inherently included into the model fit when estimating the parameters. The model fit is obtained, in case of both friction models, by the standard nonlinear least-squares minimization (Levenberg-Marquardt algorithm) of the velocity error $\|\dot{\mathbf{y}} - \hat{\dot{\mathbf{y}}}\|$, where $\hat{\dot{\mathbf{y}}}$ is the model-predicted velocity response. In case of the Maxwell-slip friction model the number of elements $N = 3$ is assumed. This renders six friction parameters to be identified and makes the model complexity, i.e. in terms of number of parameters, better comparable with that of the LuGre friction model. Note that besides the friction parameters the moving mass (inertia) is equally identified in both cases. From Figure 9, one can see that both identified friction models provide a prediction of free motion response which coincides well with experimental data. At the same time, one can see, from the zoom-in included in Figure 9, that in case of the Maxwell-slip friction model the trajectory does not converge to equilibrium but towards a stable (micro) limit cycle. This is well in accord with the analysis we made at the end of Section 3.2.

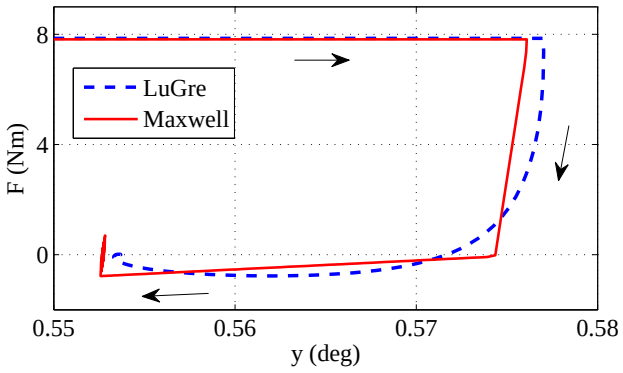

Figure 10. Friction-displacement response of the model fit of system dynamics (7) when using the LuGre and Maxwell-slip friction models. The first motion reversal (right-hand side) occurs after the system slipping with a constant Coulomb friction. The hysteresis reversal transition occurs, in case of both models, until the next motion reversal (left-hand side). The latter is followed by the attained equilibrium state. In case of Maxwell-slip friction model a micro limit cycle occurs instead of the motion stop.

Further, the pre-sliding hysteresis response of both identified models are shown in Figure 10 in the relative force-displacement coordinates. Both friction models offer nearly the same level of constant Coulomb friction until the first motion reversal (on the right-hand side). After the reversal hysteresis transitions, which are qualitatively similar but differ in the smoothness of curvature, the next motion reversal occurs (on the left-hand side) in case of both models. Close to the latter, both friction trajectories attain the final equilibrium state, while the Maxwell-slip

model provides the residual (micro) limit cycles instead of a complete motion stop.

5. Conclusions

We have analyzed and demonstrated in a numerical simulation and with experiment the damping characteristics of frictional hysteresis within the so called pre-sliding range. Based on the general consideration of friction force transitions, i.e after a motion reversal, we have compared the ideal cases of linear contact stiffness and discontinuous Coulomb friction, and the generic case of hysteresis in displacement. It has been analyzed analytically and shown in a simulation how the free motion trajectories, in all three cases, proceed towards the equilibrium. Also two dynamic friction models, e.g. LuGre and Maxwell-slip, have been taken into consideration and investigated on their nonlinear dynamics in context of a free moving mass with frictional damping. Using the Lyapunov stability theory and related tools, like Aiserman method and invariant set theorem, we have derived the conditions of asymptotic and non-asymptotic stability of relative motion with both friction models. In particularly, for the LuGre friction model the impact of contact stiffness and micro-damping parameters has been emphasized and the asymptotic stability, even without viscous friction term, has been proved. For the Maxwell-slip friction model the main result consists in deriving the criterion of asymptotic stability and analysis of occurrence of the limit cycles. Some experimental observations shown and compared with the model-based motion prediction argued in favor of the analysis made before.

References

[1] Al-Bender F, De Moerlooze K and Vanherck P 2012 *Tribology Letters* **46** 23–31
[2] Armstrong B, Dupont P and De Wit C C 1994 *Automatica* **30** 1083–1138
[3] Armstrong B and Amin B 1996 *Automatica* **32** 679–692
[4] Hensen R H, Van de Molengraft M and Steinbuch M 2003 *Automatica* **39** 2131–2137
[5] Ruderman M and Iwasaki M 2014 *International Power Electronics Conference (IPEC)* pp 1665–1670
[6] Al-Bender F and Symens W 2005 *Chaos: An Interdisciplinary Journal of Nonlinear Science* **15** 013105
[7] Armstrong B and Chen Q 2008 *IEEE Control Systems Magazine* **28** 79–89
[8] Ruderman M and Bertram T 2013 *Mechanical Systems and Signal Processing* **39** 316–332
[9] Ruderman M and Iwasaki M 2015 *IEEE Transactions on Industrial Electronics* **PP** 1–1
[10] Zabreiko P, Krasnoselskii M and Lifsic E 1970 *Soviet Math. Dokl.* **11** 73–76
[11] Wielke B 1974 *Physica status solidi (a)* **23** 237–244
[12] Grossmayer R 1979 *Journal of Sound and Vibration* **65** 353–379
[13] Alvarez J, Orlov I and Acho L 2000 *Journal of Dynamic Systems, Measurement, and Control* **122** 687–690
[14] Slotine J J and Li W 1991 *Applied Nonlinear Control* 1st ed (New Jersey, USA: Prentice Hall)
[15] Krejci P 1996 *Hysteresis, Convexity and Dissipation in Hyperbolic Equations* (Tokyo: Gattötoscho)
[16] Popov V and Gray J 2012 *ZAMM - Journal of Applied Mathematics and Mechanics* **92** 683–708
[17] De Wit C C, Olsson H, Aström K J and Lischinsky P 1995 *IEEE Trans. on automatic control* **40** 419–425
[18] Dahl P R 1968 A solid friction model TOR 158(3107-18) The Aerospace Corporation, El Segundo
[19] Aström K J and De Wit C C 2008 *IEEE Control systems magazine* **28** 101–114
[20] Lazan B J 1968 *Damping of materials and members in structural mechanics* vol 214 (Pergamon press Oxford)
[21] Iwan W D 1966 *ASME Trans., Journal of Aplied Mechanics* **33** 893–900
[22] Goldfarb M and Celanovic N 1997 *IEEE Control Systems* **17** 69–79
[23] Haessig D A and Friedland B 1991 *Journal of Dynamic Systems, Measurement, and Control* **113** 354–362
[24] Barahanov N and Ortega R 2000 *IEEE Transactions on Automatic Control* **45** 830–832
[25] Aiszerman M A and Gantmakher F R 1965 *Die absolute Stabilität von Regelsystemen* (Oldenbourg)
[26] Krasnosel'skii M and Pokrovskii A 1989 *Systems with Hysteresis* (Berlin: Springer)
[27] Brokate M and Sprekels J 1996 *Hysteresis and Phase Transitions* (Berlin: Springer)
[28] Ruderman M and Iwasaki M 2014 *IEEE International Workshop on Advanced Motion Control* pp 592–597